Penerbit Akademia Baru

Journal of Advanced Research Design

Journal homepage: http://www.akademiabaru.com/ard.html
ISSN: 2289-7984

Transient Removal of Contaminant from A Channel With Differentially Heated Wall of Cavity

Ahmat Rajab Khairul Yusri[1], Nor Azwadi Che Sidik[1,2,*]

[1] School of Mechanical Engineering, Faculty of Engineering, Universiti Teknologi Malaysia, 81310 Skudai, Johor, Malaysia
[2] Malaysia-Japan International Institute of Technology, University Teknologi Malaysia, Jalan Sultan Yahya Petra, Kampung Datuk Keramat, 54100 Kuala Lumpur, Wilayah Persekutuan Kuala Lumpur

ARTICLE INFO

Article history:
Received 15 August 2021
Received in revised form 1 November 2021
Accepted 3 November 2021
Available online 5 December 2021

Keywords:
Constrained Interpolated Profile (CIP); contaminants; cavity

ABSTRACT

This study aims to investigate the contaminants removal process from a cavity by resorting to natural flow to clean the deposits in different cavity sizes and includes different heating locations with different flow configurations. For numerical study, Constrained Interpolated Profile (CIP) method was used for the advection phase of momentum and energy equation, and central difference was used to solve the non-advection phase of momentum and energy equations. The numerical studies include different aspect ratios (AR), 1 to 4 and various Reynolds numbers (Re), 50 to 1000. It was found that a lower flowrate and larger cavity aspect ratio let the main flow to enter the cavity to the bottom without creating shear layer at end of cavity.

1. Introduction

Cavity flow can be found in flow past a panel, flow in organ pipes, flow past a sunroof of vehicle, flow past a window, flow around a weapon bay, landing gear of an aircraft and etcetera. There is a lot more applications on cavity flow such as flow over street canyon which involving environmental study related to air pollutant control.

Details on properties and effects of cavity onto main flow have been reported by many researchers such as effect of oscillation from cavity flow onto main flow [1-3], flow acoustic effect resulting from circulation past cavity as shown in Figure 1 and many more. These studies focusing on effect of cavity onto flow itself [4,5]. Parameter use for cavity flow such as depth of cavity, D and length of cavity, L will result different flow structure inside cavity. Different inlet velocity will produce different free stream velocity, U0 and different boundary layer thickness, δ. On the other hand, there is also research on contaminated cavity flow [6,7] where the contaminated cavity is studied on their particle removal process.

* *Corresponding author.*
E-mail address: azwadi@utm.my

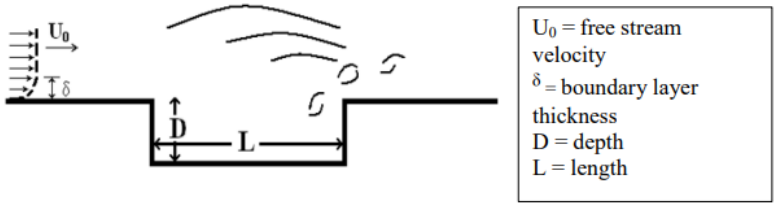

Fig.1. Geometry resulting acoustic effect on cavity flow [4]

A contaminated cavity can be seen inside hydraulic components such as metal exposed to water and resulting rust particle accumulate inside cavity [8]. Another example of a contaminated cavity is contaminated pipeline resulting from improper fitting of pipe joint. Therefore, cleaning process of the contaminated cavity becomes an important process to maintain hydraulic and pipeline to working properly. Furthermore, cleaning contaminated cavity can be a tedious process because need to dissemble them and clean them part by part.

Focusing on the poor fitting of pipeline, hydrodynamic cleaning is one of simple methods to clean the contaminated cavity without dissembling it part by part. There are many studies on hydrodynamics cleaning of components, parts and pipelines that known as one research area as a method in cleaning process in pipes. One of them is by using a restrained ball and let lateral vibration of the ball clean the wall of pipe as done by Grinis and Korin [9]. They were focusing on harvesting the levitation effect of a ball inside a pipe to clean sediment and rust inside a pipeline as shown in Figure 2. The components of the experiment as follow: item 1 is tank, item 2 is pump, item 3 is valve to control flow rate, item 4 and 8 are manometer, item 5 is flow meter, item 6 is ball used for cleaning purpose, item 7 is pipe and item 10 is flexible wire to restrain the ball. The ball will rotate due to effect of wall of pipe and provide lateral vibration of the pipe to clean the pipe.

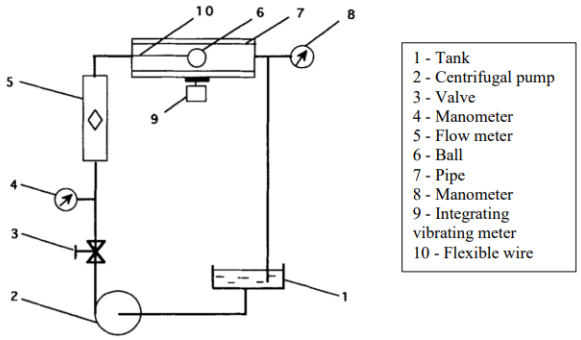

Fig. 2. Experiment equipment sketch by Grinis and Korin [7]

On the other hand, the effect of mixed convection flow in enhancing contaminant removal process is also one of the research areas in hydrodynamic cleaning in pipe. Zain [10] has studied the effect of heated bottom wall to the particle removal process from cavity. Similar study as shown in Figure 3 reported by Fang [11], where the bottom wall of cavity supplied with constant heat flux to enhance the removal process inside the cavity. The constant heat flux will change the flow structure inside cavity due to thermal buoyant effect to the fluid flow.

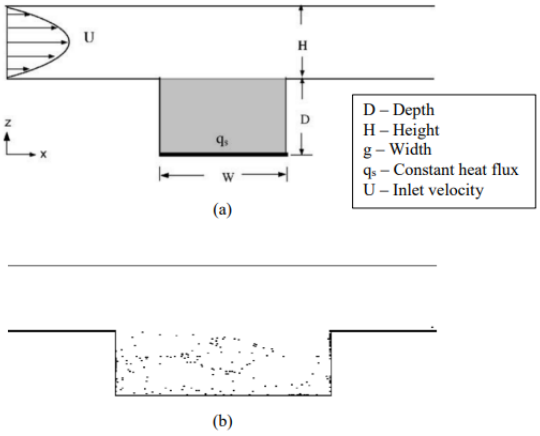

Fig. 3. Work by Fang [11] (a) Sketch of a contaminated cavity with constant heat flux at the bottom wall of cavity, (b) Remaining contaminant of cavity for aspect ratio 4 at steady state

Another examples of application-related on problem arise from flow over cavity with thermal effect is cooling computer chip and computer hardware. In order computers to function properly, cooling process of its hardware is crucial as advanced computer chip provides faster processing time but also will produce heat faster [12]. As the computer component such as processor can be costly to replace if it is burned due to overheating, cooling system for computer components is also has become an interest in the computer industry. In cooling system of computer, there are many methods such as blow cooler air to the heated component and sometimes air conditioner is used to provide faster cooling to the computer. Due to the importance of application related to flow over cavity, it is become one of interest field to further study to expanding knowledge.

Aforementioned above regarding problem arise on cavity flow, it is important to explore and study them for better understanding. In order to study on flow over the cavity, there is three methods can be used to get the results. There are 3 types of method to solve fluid dynamics which are doing analytical calculation for solution, experimental analysis and numerical method analysis [13]. For analytical calculation can be solved by some mathematical calculation by applying correct boundary and initial condition. Results obtained were due to simplification of Navier-Stokes equation and match to the real situation but it is can only apply to very simple cases such as inviscid flow. Experimental analysis is very reliable because it is done according to the real-life situation with minimal simplification and assumptions. The major concern of conducting experiment is that the test rig can be so expensive that researcher always tries to do non-destructive test to their test rig. For numerical method, it is a cheaper method to use as it can produce significant results together with the ability to control the boundary condition and parameter of study easily

Recently, Abdelmassih *et al.,* [14] have studied the flow over cavity with heated bottom wall inside the cavity by using a numerical method which is a three-dimensional direct numerical simulation and experimentally for channel flow over cavity. They have reported that there is periodic flow at Re=100 and Ri=10 in their mixed convection flow which related to heat removal process from the bottom of the cavity. Nevertheless, they captured the fluid velocity by using Particle Image Velocimetry (PIV) where small particles are seeded in the water and motion of the particles were captured and flow velocity was obtained.

There are also such similar cases study on flow over the cavity but the cavity is contaminated and hydrodynamic flow is used for contaminant removal from the cavity such as done by Fang [11]. In

this case, the heated wall inside cavity is located at the bottom wall of the cavity. His study was focused on the effect of aspect ratio of cavity and effect of Grashof number to the contaminant removal effectiveness. He found that higher Grashof number will significantly improve the contaminant removal from cavity. His study includes different aspect ratio from 0.25 to 4 and Grashof number 1 to 4000. His conclude that different flow pattern can be found by imposing heat flux from bottom of cavity. It is also shows that different aspect ratio provides different contaminant removal percentage but only limited for heated bottom wall of cavity.

In different study [15], the removal of contaminant and flow behaviour due to magnetohydrodynamic effect was studied. They were using numerical method to study the heat transfer performance and the removal process of fluid particles. In general, stronger buoyant flow is reported to improve the removal process from the cavity at higher Grashof number and higher Reynolds number. However, their report provided very limited cases which are only 3 cases for different Reynolds number and 3 cases for different Grashof number. As mixed convection flow is known by applying constant heat flux from the bottom wall of the cavity can change the flow structure, there are also right vertical wall and left vertical wall of the cavity that also can contribute to changing the flow structure. There is literature available such as the one done by Stiriba *et al.,* [16] where the right vertical wall of the cavity is remaining at constant temperature that higher than ambient temperature. Another study by Aminossadati *et al.,* [17], the heated wall is at same location but only part of the wall is heated which reported only half of the wall is heated in the middle of the wall. Their study provides data on the effect of different heated wall inside the cavity to the flow behaviour without contaminant inside the cavity.

Manca *et al.,* [18] has study numerically for temperature distribution and stream function using air for 3 different heated wall position for aspect ratio 2. Experimental study was done later by Manca et al., [19] for heated left wall of cavity. Nevertheless, they also provide experimental study for heated right wall of cavity [20]. Even though their study focused on temperature distribution, their studies also shown that different heated wall will produce different vortex structure inside cavity but their studies are limited for temperature distribution and flow structure without contaminant removal process. It also didn't include data for heated bottom wall of cavity.

It appears from the aforementioned study that investigation has been conducted regarding mixed convection cavity flow but some of their studies are more on heat removal process efficiency and flow structure inside cavity. It is appeared that removal of contaminant from cavity with mixed convection flow study can be broaden in term of different flow condition such as different Reynolds number and Grashoff number. It is also can be notify various study that used different aspect ratio of cavity and different heat source location can change the flow structure and flow behavior. Therefore, research on contaminant removal inside cavity by utilizing mixed convection flow sources from cavity wall is still a gap of knowledge in engineering and it is necessary to go for deep research on effect of Grashof number and location of heated wall to the effect of contaminant removal from the cavity. Hence, this study aims to numerically develop the flow structure in the cavity using CIP method by using streamlines plot.

2. Methodology

2.1 Governing Equations for Numerical Analysis

To simulate the flow in a channel in two-dimensional analysis, continuity equation and Navier-Stokes equation was used. There are three variables in the equation which are pressure, velocity in horizontal and vertical direction in Navier-Stokes equation. There are two popular methods used to solve the equation which is 56 primitive variable method and stream function - vorticity approach [21]. To reduce the pressure term in Navier- Stokes equation, stream function - vorticity approach is used in this research so that the variables reduce into two which is vorticity and stream function. With fewer variables in governing equation can reduce computational time to solve the equations. Stream function, ψ and vorticity, ω defined as follows

$$u = \frac{\partial \psi}{\partial y} \tag{1}$$

$$v = -\frac{\partial \psi}{\partial x} \tag{2}$$

$$\frac{\partial v}{\partial x} - \frac{\partial u}{\partial y} = \omega \tag{3}$$

For flow in channel of two-dimensional analysis, two equations will be used to solve fluid velocity which is continuity equation and Navier Stokes equation. By assuming the fluid flow is incompressible and in two dimensional, the continuity equation is expressed in Eq. (4) and Navier Stokes equation can be expressed in Eq. (5) for momentum in x-direction and Eq. (6) for momentum in Y direction.

$$\frac{\partial u}{\partial x} + \frac{\partial v}{\partial y} = 0 \tag{4}$$

$$\frac{\partial u}{\partial t} + u\frac{\partial u}{\partial x} + v\frac{\partial u}{\partial y} = -\frac{1}{\rho}\frac{\partial p}{\partial x} + \upsilon\left(\frac{\partial^2 u}{\partial x^2} + \frac{\partial^2 u}{\partial y^2}\right) \tag{5}$$

$$\frac{\partial v}{\partial t} + u\frac{\partial v}{\partial x} + v\frac{\partial v}{\partial y} = -\frac{1}{\rho}\frac{\partial p}{\partial y} + \upsilon\left(\frac{\partial^2 v}{\partial x^2} + \frac{\partial^2 v}{\partial y^2}\right) \tag{6}$$

where;
u = Velocity in the horizontal component
v = Velocity in the vertical component
p = pressure
ρ = Fluid density
υ = Kinematic viscosity

By differentiating Eq. (5) with respect to y and Eq. (6) with respect to x then subtracting these two equations will produce new equation. By using first derivative and second derivative of vorticity equation and substitute the derivatives into the new equation will produce Eq. (7) and (8) with vorticity and stream function variables include into the equation

$$\frac{\partial \omega}{\partial t} + u\frac{\partial \omega}{\partial x} + v\frac{\partial \omega}{\partial y} = -\upsilon\left(\frac{\partial^2 \omega}{\partial x^2} + \frac{\partial^2 \omega}{\partial y^2}\right) \tag{7}$$

$$\frac{\partial^2 \psi}{\partial x^2} + \frac{\partial^2 \psi}{\partial y^2} = -\omega \tag{8}$$

Dimensionless variables will be used to substitute physical variables so that input will regardless of its unit whether SI unit or metric unit. It is also used to reduce the number of physical variables and will reduce the complexity of equation [22]. To transform equation with physical quantity into dimensionless equation, these equations will be used to be substituted into Eq. (7) and (8).

$$X = \frac{x}{D} \tag{9}$$

$$Y = \frac{y}{D} \tag{10}$$

$$U = \frac{u}{u_\infty} \tag{11}$$

$$V = \frac{v}{v_\infty} \tag{12}$$

$$\Psi = \frac{\psi}{u_\infty D} \tag{13}$$

$$\Omega = \frac{\omega D}{u_\infty} \tag{14}$$

$$T = \frac{t u_\infty}{D} \tag{15}$$

$$Re = \frac{u_\infty D}{\upsilon} \tag{16}$$

By substituting, these dimensionless parameters into Eq. (7) and (8) will produce Eq. (17) and (18). It needs to emphasize that Eq. (17) consist of advection term which is a type of hyperbolic

equation and non-advection term. Advection term will be solved using Constrained Interpolated profile method (CIP) while non-advection term will be solved using central difference method.

$$\frac{\partial \Omega}{\partial T} + U\frac{\partial \Omega}{\partial X} + V\frac{\partial \Omega}{\partial Y} = \frac{1}{Re}\left(\frac{\partial^2 \Omega}{\partial X^2} + \frac{\partial^2 \Omega}{\partial Y^2}\right) \tag{17}$$

$$\frac{\partial^2 \Psi}{\partial X^2} + \frac{\partial^2 \Psi}{\partial Y^2} = -\Omega \tag{18}$$

$$\underbrace{\frac{\partial \Omega}{\partial T} + U\frac{\partial \Omega}{\partial X} + V\frac{\partial \Omega}{\partial Y}}_{\text{Advection term}} = \underbrace{\frac{1}{Re}\left(\frac{\partial^2 \Omega}{\partial X^2} + \frac{\partial^2 \Omega}{\partial Y^2}\right)}_{\text{Non-advection term}}$$

2.2 Discretization Process

The Eq. (17) will be separated into two phases which are non-advection phase at left side of the equation and right side of the equation is advection phase. It is necessary to determine the non-advection phase first and solve it using the central finite difference while the advection phase is solved using Constrained Interpolated Profile method (CIP).

The non-advection phase

$$\frac{\partial \Omega}{\partial T} = \frac{1}{\mathrm{Re}}\left(\frac{\partial^2 \Omega}{\partial X^2} + \frac{\partial^2 \Omega}{\partial Y^2}\right) = g = \text{Phase 1} \tag{19}$$

and the advection phase

$$\frac{\partial \Omega}{\partial T} + U\frac{\partial \Omega}{\partial X} + V\frac{\partial \Omega}{\partial Y} = \text{Phase 2} \tag{20}$$

2.2.1 The non-advection phase

The phase of non-advection should always be dealt with first before CIP is implemented. The non-advection phase equations are discretized using Central Finite Difference and to reduce numerical diffusion, spatial derivative of X and Y should be included as the time evolution propagate [23].

$$\frac{\partial \Omega}{\partial T} = g = \frac{1}{\mathrm{Re}}\left(\frac{\partial^2 \Omega}{\partial X^2} + \frac{\partial^2 \Omega}{\partial Y^2}\right) \tag{21}$$

$$\frac{\partial_X \Omega}{\partial T} = \partial_X g - \partial_X \Omega\frac{\partial U}{\partial X} - \partial_Y \Omega\frac{\partial V}{\partial X} \tag{22}$$

$$\frac{\partial_Y \Omega}{\partial T} = \partial_Y g - \partial_X \Omega \frac{\partial U}{\partial Y} - \partial_Y \Omega \frac{\partial V}{\partial Y} \tag{23}$$

where

$$\partial_X g = \frac{1}{\mathrm{Re}}\left(\frac{\partial^3 \Omega}{\partial X^3} + \frac{\partial^3 \Omega}{\partial X \partial Y^2}\right) \tag{24}$$

$$\partial_Y g = \frac{1}{\mathrm{Re}}\left(\frac{\partial^3 \Omega}{\partial X^2 \partial Y} + \frac{\partial^3 \Omega}{\partial Y^3}\right) \tag{25}$$

After discretization and rearrange the equation, the results from Eq. (21) are as follow

$$\frac{\partial \Omega}{\partial T} = g = \frac{1}{\mathrm{Re}}\left(\frac{\partial^2 \Omega}{\partial X^2} + \frac{\partial^2 \Omega}{\partial Y^2}\right) \tag{26}$$

$$\frac{\Omega^*_{i,j} - \Omega^n_{i,j}}{\Delta T} = \frac{1}{\mathrm{Re}}\left(\frac{\Omega^n_{i+1,j} - 2\Omega^n_{i,j} + \Omega^n_{i-1,j}}{(\Delta X)^2} + \frac{\Omega^n_{i,j+1} - 2\Omega^n_{i,j} + \Omega^n_{i,j-1}}{(\Delta Y)^2}\right) \tag{27}$$

$$\Omega^*_{i,j} = \frac{\Delta T}{\mathrm{Re}}\left(\frac{\Omega^n_{i+1,j} - 2\Omega^n_{i,j} + \Omega^n_{i-1,j}}{(\Delta X)^2} + \frac{\Omega^n_{i,j+1} - 2\Omega^n_{i,j} + \Omega^n_{i,j-1}}{(\Delta Y)^2}\right) + \Omega^n_{i,j} \tag{28}$$

For spatial derivative in X-direction, we discretize it and rearrange it as follow

$$\frac{\partial_X \Omega}{\partial T} = \partial_X g - \partial_X \Omega \frac{\partial U}{\partial X} - \partial_Y \Omega \frac{\partial V}{\partial X} \tag{29}$$

$$\frac{\partial_X \Omega^*_{i,j} - \partial_X \Omega^n_{i,j}}{\Delta T} = \partial_X g_{i,j} - \partial_X \Omega_{i,j}\left[\frac{U^n_{i+1,j} - U^n_{i-1,j}}{2\Delta X}\right] - \partial_Y \Omega_{i,j}\left[\frac{V^n_{i+1,j} - V^n_{i-1,j}}{2\Delta X}\right] \tag{30}$$

$$\partial_X \Omega^*_{i,j} = \Delta T \partial_X g_{i,j} - \Delta T \frac{\Omega^n_{i+1,j} - \Omega^n_{i-1,j}}{2\Delta X}\left[\frac{U^n_{i+1,j} - U^n_{i-1,j}}{2\Delta X}\right] - \Delta T \frac{\Omega^n_{i,j+1} - \Omega^n_{i,j-1}}{2\Delta Y}\left[\frac{V^n_{i+1,j} - V^n_{i-1,j}}{2\Delta X}\right] + \partial_X \Omega^n_{i,j} \tag{31}$$

For spatial derivative in Y-direction, we discretize it and rearrange it as follow

$$\frac{\partial_Y \Omega}{\partial T} = \partial_Y g - \partial_X \Omega \frac{\partial U}{\partial Y} - \partial_Y \Omega \frac{\partial V}{\partial Y} \tag{32}$$

$$\frac{\partial_Y \Omega^*_{i,j} - \partial_Y \Omega^n_{i,j}}{\Delta T} = \partial_Y g_{i,j} - \partial_X \Omega_{i,j} \left[\frac{U^n_{i,j+1} - U^n_{i,j-1}}{2\Delta Y} \right] - \partial_Y \Omega_{i,j} \left[\frac{V^n_{i,j+1} - V^n_{i,j-1}}{2\Delta Y} \right] \tag{33}$$

$$\partial_Y \Omega^*_{i,j} = \Delta T \partial_Y g_{i,j} - \Delta T \frac{\Omega^n_{i+1,j} - \Omega^n_{i-1,j}}{2\Delta X} \left[\frac{U^n_{i,j+1} - U^n_{i,j-1}}{2\Delta Y} \right] - \Delta T \frac{\Omega^n_{i,j+1} - \Omega^n_{i,j-1}}{2\Delta Y} \left[\frac{V^n_{i,j+1} - V^n_{i,j-1}}{2\Delta Y} \right] + \partial_Y \Omega^n_{i,j} \tag{34}$$

The spatial derivative for X dimensionless direction and Y dimensionless direction for phase one will discretize and rearrange it as follow

$$\partial_X g = \frac{1}{\mathrm{Re}} \left(\frac{\partial^3 \Omega}{\partial X^3} + \frac{\partial^3 \Omega}{\partial X \partial Y^2} \right) \tag{35}$$

$$\partial_X \Omega_{i,j} = \frac{1}{\mathrm{Re}} \left[\left(\frac{\Omega^n_{i+2,j} - 2\Omega^n_{i+1,j} + 2\Omega^n_{i-1,j} - \Omega^n_{i-2,j}}{2\Delta X^3} \right) + \left(\frac{\Omega^n_{i+1,j+1} - 2\Omega^n_{i+1,j} + \Omega^n_{i+1,j-1} - \Omega^n_{i-1,j+1} + 2\Omega^n_{i-1,j} - \Omega^n_{i-1,j-1}}{2\Delta X (\Delta Y)^2} \right) \right] \tag{36}$$

$$\partial_Y g = \frac{1}{\mathrm{Re}} \left(\frac{\partial^3 \Omega}{\partial X^2 \partial Y} + \frac{\partial^3 \Omega}{\partial Y^3} \right) \tag{37}$$

$$\partial_Y \Omega_{i,j} = \frac{1}{\mathrm{Re}} \left[\left(\frac{\Omega^n_{i+1,j+1} - 2\Omega^n_{i,j+1} + \Omega^n_{i-1,j+1} - \Omega^n_{i+1,j-1} + 2\Omega^n_{i,j-1} - \Omega^n_{i-1,j-1}}{2\Delta Y (\Delta X)^2} \right) + \left(\frac{\Omega^n_{i,j+2} - 2\Omega^n_{i,j+1} + 2\Omega^n_{i,j-1} - \Omega^n_{i,j-2}}{2\Delta Y^3} \right) \right] \tag{38}$$

By combining these equations for X-direction and Y-direction will produce

$$\partial_X \Omega^*_{i,j} = \partial_X \Omega^n_{i,j} - \Delta T \frac{\Omega^n_{i+1,j} - \Omega^n_{i-1,j}}{2\Delta X}\left[\frac{U^n_{i+1,j} - U^n_{i-1,j}}{2\Delta X}\right] - \Delta T \frac{\Omega^n_{i,j+1} - \Omega^n_{i,j-1}}{2\Delta Y}\left[\frac{V^n_{i+1,j} - V^n_{i-1,j}}{2\Delta X}\right]$$
$$+ \frac{\Delta T}{\mathrm{Re}}\left(\frac{\Omega^n_{i+2,j} - 2\Omega^n_{i+1,j} + 2\Omega^n_{i-1,j} - \Omega^n_{i-2,j}}{2\Delta X^3} + \frac{\Omega^n_{i+1,j+1} - 2\Omega^n_{i+1,j} + \Omega^n_{i+1,j-1} - \Omega^n_{i-1,j+1} + 2\Omega^n_{i-1,j} - \Omega^n_{i-1,j-1}}{2\Delta X(\Delta Y)^2}\right) \quad (39)$$

$$\partial_Y \Omega^*_{i,j} = \partial_Y \Omega^n_{i,j} - \Delta T \frac{\Omega^n_{i+1,j} - \Omega^n_{i-1,j}}{2\Delta X}\left[\frac{U^n_{i,j+1} - U^n_{i,j-1}}{2\Delta Y}\right] - \Delta T \frac{\Omega^n_{i,j+1} - \Omega^n_{i,j-1}}{2\Delta Y}\left[\frac{V^n_{i,j+1} - V^n_{i,j-1}}{2\Delta Y}\right]$$
$$+ \frac{\Delta T}{\mathrm{Re}}\left(\frac{\Omega^n_{i+1,j+1} - 2\Omega^n_{i,j+1} + \Omega^n_{i-1,j+1} - \Omega^n_{i+1,j-1} + 2\Omega^n_{i,j-1} - \Omega^n_{i-1,j-1}}{2\Delta Y(\Delta X)^2} + \frac{\Omega^n_{i,j+2} - 2\Omega^n_{i,j+1} + 2\Omega^n_{i,j-1} - \Omega^n_{i,j-2}}{2\Delta Y^3}\right) \quad (40)$$

Noted that $\Omega^*_{i,j}$ is the value obtained from non-advection phase. From here, these values will be used to restore the value for the following time step. However, to accommodate few values that can be observed in the last two equations, the unique procedure closes the wall should be performed [20]. These values are $\Omega^n_{i+2,j}$, $\Omega^n_{i-2,j}$, $\Omega^n_{i,j+2}$ and $\Omega^n_{i,j-2}$. For example, at the point i=2, $\Omega^n_{i-2,j} = \Omega^n_{0,j}$ and there was no such point in MATLAB, therefore procedure is based on the average value of the neighbouring nodes

$$\frac{\Omega^n_{2,j} + \Omega^n_{0,j}}{2} = \Omega^n_{1,j} \quad (41)$$

$$\Omega^n_{0,j} = 2\Omega^n_{1,j} - \Omega^n_{2,j} \quad (42)$$

$$\frac{\Omega^n_{\max i-1,j} + \Omega^n_{\max i+1,j}}{2} = \Omega^n_{\max i,j} \quad (43)$$

$$\Omega^n_{\max i+1,j} = 2\Omega^n_{\max i,j} - \Omega^n_{\max i-1,j} \quad (44)$$

$$\frac{\Omega^n_{i,0} + \Omega^n_{i,2}}{2} = \Omega^n_{i,1} \quad (45)$$

$$\Omega^n_{i,0} = 2\Omega^n_{i,1} - \Omega^n_{i,2} \quad (46)$$

$$\frac{\Omega^n_{i,\max j-1} + \Omega^n_{i,\max j+1}}{2} = \Omega^n_{i,\max j} \quad (47)$$

$$\Omega^n_{i,\max j+1} = 2\Omega^n_{i,\max j} - \Omega^n_{i,\max j-1} \tag{48}$$

In MATLAB, this following statement can be used to overcome the near-wall treatment.

IF $i = (\max i - 1)$, $B1 = 2\Omega^n_{\max i,j} - \Omega^n_{\max i-1,j}$ ELSE, $B1 = \Omega^n_{i+2,j}$

IF $i = 2$, $B2 = 2\Omega^n_{1,j} - \Omega^n_{2,j}$ ELSE, $B2 = \Omega^n_{i-2,j}$

IF $j = (\max j - 1)$, $B3 = 2\Omega^n_{i,\max j} - \Omega^n_{i,\max j-1}$ ELSE, $B3 = \Omega^n_{i,j+2}$

IF $j = 2$, $B4 = 2\Omega^n_{i,1} - \Omega^n_{i,2}$ ELSE $B4 = \Omega^n_{i,j-2}$

Then, the equation can be rewritten as

$$\partial_X \Omega^*_{i,j} = \partial_X \Omega^n_{i,j} - \Delta T \frac{\Omega^n_{i+1,j} - \Omega^n_{i-1,j}}{2\Delta X}\left[\frac{U^n_{i+1,j} - U^n_{i-1,j}}{2\Delta X}\right] - \Delta T \frac{\Omega^n_{i,j+1} - \Omega^n_{i,j-1}}{2\Delta Y}\left[\frac{V^n_{i+1,j} - V^n_{i-1,j}}{2\Delta X}\right] + \frac{\Delta T}{\mathrm{Re}}\left(\frac{B1 - 2\Omega^n_{i+1,j} + 2\Omega^n_{i-1,j} - B2}{2\Delta X^3} + \frac{\Omega^n_{i+1,j+1} - 2\Omega^n_{i+1,j} + \Omega^n_{i+1,j-1} - \Omega^n_{i-1,j+1} + 2\Omega^n_{i-1,j} - \Omega^n_{i-1,j-1}}{2\Delta X(\Delta Y)^2}\right) \tag{49}$$

$$\partial_Y \Omega^*_{i,j} = \partial_Y \Omega^n_{i,j} - \Delta T \frac{\Omega^n_{i+1,j} - \Omega^n_{i-1,j}}{2\Delta X}\left[\frac{U^n_{i,j+1} - U^n_{i,j-1}}{2\Delta Y}\right] - \Delta T \frac{\Omega^n_{i,j+1} - \Omega^n_{i,j-1}}{2\Delta Y}\left[\frac{V^n_{i,j+1} - V^n_{i,j-1}}{2\Delta Y}\right] + \frac{\Delta T}{\mathrm{Re}}\left(\frac{B3 - 2\Omega^n_{i,j+1} + 2\Omega^n_{i,j-1} - B4}{2\Delta Y^3} + \frac{\Omega^n_{i+1,j+1} - 2\Omega^n_{i,j+1} + \Omega^n_{i-1,j+1} - \Omega^n_{i+1,j-1} + 2\Omega^n_{i,j-1} - \Omega^n_{i-1,j-1}}{2\Delta Y(\Delta X)^2}\right) \tag{50}$$

2.2.2 The advection phase

CIP will be executed in this chapter for solving advection equation mention earlier. The cubic polynomial in the two-dimensional hyperbolic equation is using rectangular grid as discussed by Ref. [18]

$$\begin{aligned}\upsilon_{i,j}(X,Y) = {} & \left[\left(A1_{i,j}\hat{X} + A2_{i,j}\hat{Y} + A3_{i,j}\right)\hat{X} + A4_{i,j}\hat{Y}\right. \\ & \left. + \partial_X \Omega_{i,j}\right]\hat{X} \\ & + \left[\left(A5_{i,j}\hat{Y} + A6_{i,j}\hat{X} + A7_{i,j}\right)\hat{Y} + \partial_Y \Omega_{i,j}\right]\hat{Y} \\ & + \Omega_{i,j}\end{aligned} \tag{51}$$

where $\hat{X}$ = X-$X_{i,j}$ and $\hat{Y}$ = Y-$Y_{i,j}$. The following parameters are incorporated in CIP method in determining the value of Ω(X,Y)

$$A8_{i,j} = \Omega_{i,j} - \Omega_{i+1,j} - \Omega_{i,j+1} + \Omega_{i+1,j+1} \tag{52}$$

$$A1_{i,j} = \left[-2d_i + \partial_X \left(\Omega_{i+1,j} + \Omega_{i,j}\right)\Delta X\right] / \Delta X^3 \tag{53}$$

$$A2_{i,j} = \left[A8_{i,j} - \partial_X d_j \Delta X\right] / \left(\Delta X^2 \Delta Y\right) \tag{54}$$

$$A3_{i,j} = \left[3d_i - \partial_X \left(\Omega_{i+1,j} + 2\Omega_{i,j}\right)\Delta X\right] / \left(\Delta X \Delta Y\right) \tag{55}$$

$$A4_{i,j} = \left[-A8_{i,j} + \partial_X d_j \Delta X + \partial_Y d_i \Delta Y\right] / \left(\Delta X \Delta Y\right) \tag{56}$$

$$A5_{i,j} = \left[-2d_j + \partial_Y \left(\Omega_{i,j+1} + \Omega_{i,j}\right)\Delta Y\right] / \Delta Y^3 \tag{57}$$

$$A6_{i,j} = \left[A8_{i,j} - \partial_Y d_i \Delta Y\right] / \left(\Delta X \Delta Y^2\right) \tag{58}$$

$$A7_{i,j} = \left[3d_j - \partial_Y \left(\Omega_{i,j+1} + 2\Omega_{i,j}\right)\Delta Y\right] / \Delta Y^2 \tag{59}$$

The solution for Ω , $\partial_X \Omega$ and $\partial_Y \Omega$ after period of ΔT can be estimated and after the one-time step of ΔT where $\Omega_{\mathrm{I,j}}^{n+1} = \mho_{\mathrm{I,j}}(\mathrm{X_{I,j}} - U\Delta T, \mathrm{Y_{I,j}} - \mathrm{V}\Delta\mathrm{T}), \partial_{\mathrm{X}}\theta_{\mathrm{i,j}}^{n+1} = \partial_{\mathrm{X}}\mho_{\mathrm{i,j}}$ and $\partial_{\mathrm{Y}}\Omega_{\mathrm{i,j}}^{n+1} = \partial_{\mathrm{Y}}\mho_{\mathrm{i,j}}$ can be rearrange explicitly as

$$\begin{aligned}\Omega_{i,j}^{n+1} = &\left[\left(A1_{i,j}\xi + A2_{i,j}\eta + A3_{i,j}\right)\xi + A4_{i,j}\eta + \partial_X \Omega_{i,j}^{*}\right] \\ &+ \left[\left(A5_{i,j}\eta + A6_{i,j}\xi + A7_{i,j}\right)\eta + \partial_Y \Omega_{i,j}^{*}\right]\eta + \Omega_{i,j}^{*}\end{aligned} \tag{60}$$

$$\begin{aligned}\partial_X \Omega_{i,j}^{n+1} = &\left(3A1_{i,j}\xi + 2A2_{i,j}\eta + 2A3_{i,j}\right)\xi \\ &+ \left(A4_{i,j} + A6_{i,j}\eta\right)\eta + \partial_X \Omega_{i,j}^{*}\end{aligned} \tag{61}$$

$$\begin{aligned}\partial_Y \Omega_{i,j}^{n+1} = &\left(3A5_{i,j}\eta + 2A6_{i,j}\xi + 2A7_{i,j}\right)\eta \\ &+ \left(A4_{i,j} + A2_{i,j}\xi\right)\xi + \partial_Y \Omega_{i,j}^{*}\end{aligned} \tag{62}$$

where $\eta = -\Delta$V T, $\xi = -\Delta$ U T. The Eq. above is obtained for U < 0 and V < 0 as defined in Figure 4 which is the upper left mesh. Thus, depending on the sign of U and V, i+1→i-1, ΔY= $-\Delta$X and for U ≥ 0 and, j+1→ J-1, ΔY= -ΔY for V ≥ 0. The following technique should be followed to optimize the codes.

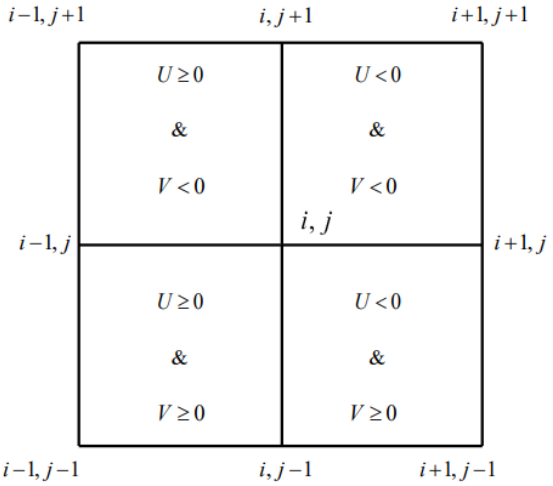

Fig. 4. Meshing of CIP in two dimensional

$$YY = -V\Delta T$$
$$XX = -U\Delta T$$
$$jsgn = sign(V)$$
$$isgn = sign(U)$$
$$im = i - isgn$$
$$jm = j - jsign$$
$$d_i = \Omega_{i+1,j} - \Omega_{i,j}$$
$$d_j = \Omega_{i,j+1} - \Omega_{i,j}$$

The treatment of grid cell will be substituted into the equation earlier to coefficient so that the coefficient is written as follow

$$A8 = \Omega_{i,j} - \Omega_{im1,j} - \Omega_{i,jm1} + \Omega_{im1,jm1} \tag{63}$$

$$A1_{i,j} = \frac{-2(\Omega_{im1,j} - \Omega_{i,j}) + \left(\partial_X \Omega_{im1,j} + \partial_X \Omega_{i,j}\right)\Delta X \times (-i\,\mathrm{sgn})}{\Delta X^3 \times (-i\,\mathrm{sgn})} \tag{64}$$

$$A2_{i,j} = \frac{A8_{i,j} - \left(\partial_X \Omega_{i,jm1} + \partial_X \Omega_{i,j}\right)\Delta X \times (-i\,\mathrm{sgn})}{\left(\Delta X^2 \Delta Y\right) \times (-j\,\mathrm{sgn})} \tag{65}$$

$$A3_{i,j} = \frac{3(\Omega_{im1,j} - \Omega_{i,j}) - \left(\partial_X \Omega_{im1,j} + 2\partial_X \Omega_{i,j}\right)\Delta X \times (-i\,\mathrm{sgn})}{\Delta X^2} \tag{66}$$

$$A4_{i,j} = \frac{-A2_{i,j}\left(\Delta X^2\right) + \left(\partial_Y \Omega_{im1,j} - \partial_Y \Omega_{i,j}\right)}{\Delta X \times (-i\,\mathrm{sgn})} \tag{67}$$

$$A5_{i,j} = \frac{-2(\Omega_{i,jm1} - \Omega_{i,j}) + \left(\partial_Y \Omega_{i,jm1} + \partial_Y \Omega_{i,j}\right)\Delta Y \times (-j\,\mathrm{sgn})}{\Delta Y^3 \times (-j\,\mathrm{sgn})} \tag{68}$$

$$A6_{i,j} = \frac{A8_{i,j} - \left(\partial_Y \Omega_{im1,j} - \partial_Y \Omega_{i,j}\right)\Delta Y \times (-j\,\mathrm{sgn})}{\left(\Delta X \Delta Y^2\right) \times (-i\,\mathrm{sgn})} \tag{69}$$

$$A7_{i,j} = \frac{3(\Omega_{i,jm1} - \Omega_{i,j}) - \left(\partial_Y \Omega_{i,jm1} + 2\partial_Y \Omega_{i,j}\right)\Delta Y \times (-j\,\mathrm{sgn})}{\Delta Y^2} \tag{70}$$

$$\Omega_{i,j}^{n+1} = \left[\left(A1_{i,j} XX + A2_{i,j} YY + A3_{i,j}\right) XX + A4_{i,j} YY + \partial_X \Omega_{i,j}^{*}\right] XX + \left[\left(A5_{i,j} YY + A6_{i,j} XX + A7_{i,j}\right) YY + \partial_Y \Omega_{i,j}^{*}\right] YY + \Omega_{j,3}^{*} \tag{71}$$

$$\partial_X \Omega_{i,j}^{n+1} = \left(3A1_{i,j} XX + 2A2_{i,j} YY + 2A3_{i,j}\right) XX + \left(A4_{i,j} + A6_{i,j} YY\right) YY + \partial_X \Omega_{i,j}^{*} \tag{72}$$

$$\partial_Y \Omega_{i,j}^{n+1} = \left(3A5_{i,j} YY + 2A6_{i,j} XX + 2A7_{i,j}\right) YY + \left(A4_{i,j} + A2_{i,j} XX\right) XX + \partial_Y \Omega_{i,j}^{*} \tag{73}$$

2.3 Drag Force Equation for Contaminants Trajectory

Contaminant will be added inside the cavity as small particles where the trajectory of these particles will be determined by using equation of motion. Drag force will be determined in this research as other components such as buoyancy and lift force are negligible in this study. The fluid and particles will be treated as Eulerian-Langrangian approach where the particle is treated as a point force and the fluid will influence the particle motion. Similar fluid and particles density is applied in the simulation codes (density = 1000kg/m^3). Drag force is defined as following and the discretization is as Eq. (75)

$$m_p \frac{dv_p}{dt} = f_d \tag{74}$$

$$m_p \frac{v_p^{n+1} - v_p^n}{\Delta t} = f_d \tag{75}$$

where,
mp = Mass of particle
$vp\ n$+1 = velocity of the particle at time n+1
$vp\ n$ = velocity of the particle at time n
Δt = time step
fd = drag force

The location of particles after time projection will be defined by using equation of motion as follow

$$v_p^{n+1} = \frac{x_p^{n+1} - x_p^n}{\Delta t} \tag{76}$$

$$x_p^{n+1} = v_p^{n+1}\Delta t + x_p^n \tag{77}$$

The drag force of the particle can be defined as Eq. (78)

$$f_d = C_d A_p \rho \frac{|u - v_j|(u - v_j)}{2} \tag{78}$$

$$C_d = \frac{24}{Re_p} \tag{79}$$

$$Re_p = \frac{D_p|V|}{\upsilon} \tag{80}$$

where;
fd = Drag force
Cd = Drag coefficient
Ap = Area of particle
Dp = Diameter of particle
$|V|$ = Relative velocity between fluid and particle

2.4 Mixed Convection with The Differently Heated Wall of Cavity

For mixed convection flow, a wall of cavity will be heated with constant temperature and the other walls are adiabatic. The governing equation for momentum has slightly different from isothermal cases. There is additional term will be included as temperature gradient will be included in the momentum equation. Another equation also will be used for solving mixed convection flow which is energy equation. This equation turns into dimensionless variables and the process is same as isothermal derivation as mention earlier. The dimensionless variables of momentum equation and energy equation are mentioned below.

Dimensionless momentum equation

$$\frac{\partial \Omega}{\partial T} + U\frac{\partial \Omega}{\partial X} + V\frac{\partial \Omega}{\partial Y} = \frac{1}{Re}\left(\frac{\partial^2 \Omega}{\partial X^2} + \frac{\partial^2 \Omega}{\partial Y^2}\right) + \frac{Gr}{Re^2}\frac{\partial \theta}{\partial X} \tag{81}$$

Dimensionless energy equation

$$\frac{\partial \theta}{\partial T} + U\frac{\partial \theta}{\partial X} + V\frac{\partial \theta}{\partial Y} = \frac{1}{PrRe}\left(\frac{\partial^2 \theta}{\partial X^2} + \frac{\partial^2 \theta}{\partial Y^2}\right) \tag{82}$$

where

$$\theta = \frac{\mathrm{T} - \mathrm{T}_c}{\mathrm{T}_H - \mathrm{T}_c} \tag{78}$$

The advection phase for the momentum equation remains the same as in isothermal case but the non-advection phase for the momentum equation will have some adjustment to satisfy the additional term in the equation. For energy equation, the advection term will solve based on Eq. (79)-(81)

$$\frac{\partial \theta}{\partial T} = -\left(U\frac{\partial \theta}{\partial X} + V\frac{\partial \theta}{\partial Y}\right) \tag{79}$$

$$\frac{\partial_x \theta}{\partial T} = -\left(U\frac{\partial_x \theta}{\partial X} + V\frac{\partial_x \theta}{\partial Y}\right) \tag{80}$$

$$\frac{\partial_Y \theta}{\partial T} = -\left(U\frac{\partial_Y \theta}{\partial X} + V\frac{\partial_Y \theta}{\partial Y}\right) \tag{81}$$

For non-advection phase, the momentum equation is solved based on Eq. (82)-(84) and energy equation will be solved by using Eq. (85)-(87). These equations are still needed to have near-wall treatment as mentioned earlier in isothermal section.

$$\frac{\partial \Omega}{\partial T} = \frac{1}{Re}\left(\frac{\partial^2 \Omega}{\partial X^2} + \frac{\partial^2 \Omega}{\partial Y^2}\right) + \frac{Gr}{Re^2}\frac{\partial \theta}{\partial X} \tag{82}$$

$$\frac{\partial_X \Omega}{\partial T} = \frac{1}{Re}\left(\frac{\partial^3 \Omega}{\partial X^3} + \frac{\partial^3 \Omega}{\partial X \partial Y^2}\right) - \partial_X \Omega\frac{\partial U}{\partial X} - \partial_Y \Omega\frac{\partial V}{\partial X} + \frac{Gr}{Re^2}\partial_X \frac{\partial \theta}{\partial X} \tag{83}$$

$$\frac{\partial_Y \Omega}{\partial T} = \frac{1}{Re}\left(\frac{\partial^3 \Omega}{\partial X^2 \partial Y} + \frac{\partial^3 \Omega}{\partial Y^3}\right) - \partial_X \Omega\frac{\partial U}{\partial Y} - \partial_Y \Omega\frac{\partial V}{\partial Y} + \frac{Gr}{Re^2}\partial_X \frac{\partial \theta}{\partial Y} \tag{84}$$

$$\frac{\partial \theta}{\partial T} = \frac{1}{PrRe}\left(\frac{\partial^2 \theta}{\partial X^2} + \frac{\partial^2 \theta}{\partial Y^2}\right) \tag{85}$$

$$\frac{\partial_X \theta}{\partial T} = \frac{1}{PrRe}\left(\frac{\partial^3 \theta}{\partial X^3} + \frac{\partial^3 \theta}{\partial X \partial Y^2}\right) - \partial_X \theta \frac{\partial U}{\partial X} - \partial_Y \theta \frac{\partial V}{\partial X} \tag{86}$$

$$\frac{\partial_Y \theta}{\partial T} = \frac{1}{PrRe}\left(\frac{\partial^3 \theta}{\partial X^2 \partial Y} + \frac{\partial^3 \theta}{\partial Y^3}\right) - \partial_X \theta \frac{\partial U}{\partial Y} - \partial_Y \theta \frac{\partial V}{\partial Y} \tag{87}$$

After discretization, the results from Eq. (62)-(84) yields
From Eq. (62)

$$\frac{\Omega_{i,j}^* - \Omega_{i,j}^n}{\Delta T} = \frac{1}{Re}\left(\frac{\Omega_{i+1,j}^n - 2\Omega_{i,j}^n + \Omega_{i-1,j}^n}{(\Delta X)^2} + \frac{\Omega_{i,j+1}^n - 2\Omega_{i,j}^n + \Omega_{i,j-1}^n}{(\Delta Y)^2}\right) + \frac{Gr}{Re^2}\left(\frac{\theta_{i+1,j}^n - \theta_{i-1,j}^n}{2\Delta X}\right) \tag{88}$$

Rearrangement the equation to

$$\Omega_{i,j}^* = \Omega_{i,j}^n + \frac{\Delta T}{Re}\left(\frac{\Omega_{i+1,j}^n - 2\Omega_{i,j}^n + \Omega_{i-1,j}^n}{(\Delta X)^2} + \frac{\Omega_{i,j+1}^n - 2\Omega_{i,j}^n + \Omega_{i,j-1}^n}{(\Delta Y)^2}\right) + \frac{\Delta T Gr}{Re^2}\left(\frac{\theta_{i+1,j}^n - \theta_{i-1,j}^n}{2\Delta X}\right) \tag{89}$$

From Eq. (63)

$$\frac{\partial_X \Omega_{i,j}^* - \partial_X \Omega_{i,j}^n}{\Delta T} = \frac{1}{Re}\left(\frac{\Omega_{i+2,j}^n - 2\Omega_{i+1,j}^n + 2\Omega_{i-1,j}^n - \Omega_{i-2,j}^n}{2\Delta X^3} + \frac{\Omega_{i+1,j+1}^n - 2\Omega_{i+1,j}^n + \Omega_{i+1,j-1}^n - \Omega_{i-1,j+1}^n + 2\Omega_{i-1,j}^n - \Omega_{i-1,j-1}^n}{2\Delta X(\Delta Y)^2}\right) - \partial_X \Omega_{i,j} \frac{U_{i+1,j}^n - U_{i-1,j}^n}{2\Delta X} - \partial_Y \Omega_{i,j} \frac{V_{i,+1j}^n - V_{i-1,j}^n}{2\Delta X} + \frac{Gr}{Re^2}\left(\frac{\theta_{i+1,j}^n - 2\theta_{i,j}^n + \theta_{i-1,j}^n}{(\Delta X)^2}\right)$$

After arrangement

$$\begin{aligned}
&\partial_X \Omega^*_{i,j} \\
&= \partial_X \Omega^n_{i,j} + \frac{\Delta T}{Re}\left(\frac{\Omega^n_{i+2,j} - 2\Omega^n_{i+1,j} + 2\Omega^n_{i-1,j} - \Omega^n_{i-2,j}}{2\Delta X^3}\right. \\
&\left. + \frac{\Omega^n_{i+1,j+1} - 2\Omega^n_{i+1,j} + \Omega^n_{i+1,j-1} - \Omega^n_{i-1,j+1} + 2\Omega^n_{i-1,j} - \Omega^n_{i-1,j-1}}{2\Delta X(\Delta Y)^2}\right) \\
&- \left(\frac{\Omega^n_{i+1,j} - \Omega^n_{i-1,j}}{2\Delta X}\right)\frac{U^n_{i+1,j} - U^n_{i-1,j}}{2\Delta X}\Delta T \\
&- \left(\frac{\Omega^n_{i,j+1} - \Omega^n_{i,j-1}}{2\Delta Y}\right)\frac{V^n_{i+1,j} - V^n_{i-1,j}}{2\Delta X}\Delta T \\
&+ \frac{Gr}{Re^2}\left(\frac{\theta^n_{i+1,j} - 2\theta^n_{i,j} + \theta^n_{i-1,j}}{(\Delta X)^2}\right)\Delta T
\end{aligned} \tag{90}$$

From Eq. (64)

$$\begin{aligned}
&\frac{\partial_Y \Omega^*_{i,j} - \partial_Y \Omega^n_{i,j}}{\Delta \mathrm{T}} \\
&= \frac{1}{Re}\left(\frac{\Omega^n_{i+1,j+1} - 2\Omega^n_{i,j+1} + \Omega^n_{i-1,j+1} - \Omega^n_{i+1,j-1} + 2\Omega^n_{i,j-1} - \Omega^n_{i-1,j-1}}{2\Delta Y(\Delta X)^2}\right. \\
&\left. + \frac{\Omega^n_{i,j+2} - 2\Omega^n_{i,j+1} + 2\Omega^n_{i,j-1} - \Omega^n_{i,j-2}}{2\Delta Y^3}\right) - \partial_X \Omega_{i,j}\frac{U^n_{i,j+1} - U^n_{i,j-1}}{2\Delta Y} \\
&- \partial_Y \Omega_{i,j}\frac{V^n_{i,j+1} - V^n_{i,j-1}}{2\Delta Y} \\
&+ \frac{Gr}{Re^2}\left(\frac{\theta^n_{i+1,j+1} - \theta^n_{i+1,j-1} - \theta^n_{i-1,j+1} + \theta^n_{i-1,j-1}}{4\Delta X\Delta Y}\right)
\end{aligned} \tag{91}$$

After arrangement

$$\begin{aligned}
&\partial_Y \Omega^*_{i,j} \\
&= \partial_Y \Omega^n_{i,j} + \frac{\Delta T}{Re}\left(\frac{\Omega^n_{i,j+2} - 2\Omega^n_{i,j+1} + 2\Omega^n_{i,j-1} - \Omega^n_{i,j-2}}{2\Delta Y^3}\right. \\
&\left. + \frac{\Omega^n_{i+1,j+1} - 2\Omega^n_{i,j+1} + \Omega^n_{i-1,j+1} - \Omega^n_{i+1,j-1} + 2\Omega^n_{i,j-1} - \Omega^n_{i-1,j-1}}{2\Delta Y(\Delta X)^2}\right) \\
&- \left(\frac{\Omega^n_{i+1,j} - \Omega^n_{i-1,j}}{2\Delta X}\right)\frac{U^n_{i,j+1} - U^n_{i,j-1}}{2\Delta Y}\Delta T \\
&- \left(\frac{\Omega^n_{i,j+1} - \Omega^n_{i,j-1}}{2\Delta Y}\right)\frac{V^n_{i,j+1} - V^n_{i,j-1}}{2\Delta Y}\Delta T \\
&+ \frac{Gr}{Re^2}\left(\frac{\theta^n_{i+1,j+1} - \theta^n_{i+1,j-1} - \theta^n_{i-1,j+1} + \theta^n_{i-1,j-1}}{4\Delta X\Delta Y}\right)\Delta T
\end{aligned} \tag{92}$$

For the advection stage, the constrained polynomial is used to approximate the spatial quantities of the grid interval using its neighbouring grid point's spatial derivative value. This process is similar for advection phase of isothermal section. For the energy equation, the advection phase describes as follow

$$\vartheta_{i,j}(X,Y) = \left[\left(B1_{i,j}\hat{X} + B2_{i,j}\hat{Y} + B3_{i,j}\right)\hat{X} + B4_{i,j}\hat{Y} + \partial_X\theta_{i,j}\right]\hat{X} + \left[\left(B5_{i,j}\hat{Y} + B6_{i,j}\hat{X} + B7_{i,j}\right)\hat{Y} + \partial_Y\theta_{i,j}\right]\hat{Y} + \theta_{i,j} \quad (93)$$

where $\hat{X}$ = X-$X_{i,j}$ and $\hat{Y}$ = Y-$Y_{i,j}$. The coefficients were determined so that the interpolation function and its first derivatives were continuous at both ends. With this restriction, the numerical diffusion can be greatly reduced when the interpolated profile was constructed. To determine the value of θ (X, Y) the parameters as following are integrated into CIP method

$$B8_{i,j} = \theta_{i,j} - \theta_{i+1,j} - \theta_{i,j+1} + \theta_{i+1,j+1} \quad (94)$$

$$B1_{i,j} = \left[-2e_i + \partial_X\left(\theta_{i+1,j} + \theta_{i,j}\right)\Delta X\right]/\Delta X^3 \quad (95)$$

$$B2_{i,j} = \left[A8_{i,j} - \partial_X e_j \Delta X\right]/(\Delta X^2 \Delta Y) \quad (96)$$

$$B3_{i,j} = \left[3e_i - \partial_X\left(\Omega_{i+1,j} + 2\theta_{i,j}\right)\Delta X\right]/\Delta X^2 \quad (97)$$

$$B4_{i,j} = \left[-A8_{i,j} + \partial_X e_j \Delta X + \partial_Y d_i \Delta Y\right]/(\Delta X \Delta Y) \quad (98)$$

$$B5_{i,j} = \left[-2e_j + \partial_Y\left(\theta_{i,j+1} + \theta_{i,j}\right)\Delta Y\right]/\Delta Y^3 \quad (99)$$

$$B6_{i,j} = \left[A8_{i,j} - \partial_Y e_i \Delta Y\right]/(\Delta X \Delta Y^2) \quad (100)$$

$$B7_{i,j} = \left[3e_j - \partial_Y\left(\theta_{i,j+1} + 2\theta_{i,j}\right)\Delta Y\right]/\Delta Y^2 \quad (101)$$

After period of time, ΔT, the solution for θ, $\partial_X\theta$ and $\partial_Y\theta$ also can be predicted and after the one-time step of ΔT where $\Omega_{i,j}^{n+1} = \vartheta_{i,j}(X_{i,j} - U\Delta T, Y_{i,j} - U\Delta T)$, $\partial_X\theta_{i,j}^{n+1} = \partial_X\vartheta_{i,j}$ and $\partial_Y\theta_{i,j}^{n+1} = \partial_Y\vartheta_{i,j}$ can be written explicitly as

$$\theta_{i,j}^{n+1} = \left[(B1_{i,j}\xi + B2_{i,j}\eta + B3_{i,j})\xi + B4_{i,j}\eta + \partial_X\theta_{i,j}^{*}\right]\xi + \left[(B5_{i,j}\eta + B6_{i,j}\xi + B7_{i,j})\eta + \partial_Y\theta_{i,j}^{*}\right]\eta + \Omega_{i,j}^{*} \quad (102)$$

$$\partial_X\theta_{i,j}^{n+1} = (3\,B1_{i,j}\xi + 2\,B2_{i,j}\eta + 2\,B3_{i,j})\xi + (B4_{i,j} + B6_{i,j}\eta)\eta + \partial_X\theta_{i,j}^{*} \quad (103)$$

$$\partial_Y\theta_{i,j}^{n+1} = (3\,B5_{i,j}\eta + 2\,B6_{i,j}\xi + 2\,B7_{i,j})\eta + (B4_{i,j} + B2_{i,j}\xi)\xi + \partial_Y\theta_{i,j}^{*} \quad (104)$$

where $\xi = -U\Delta T$, $\eta = -V\Delta T$. The Eq. (48) to Eq. (50) is derived for $U < 0$ and $V < 0$ as described in Figure 5, which is the upper right cell. Thus, depending on the value of U and V, $i + 1 \rightarrow i - 1$, $\Delta X = -\Delta X$ and for $U \geq 0$ and, $j + 1 \rightarrow j - 1$, $\Delta Y = -\Delta Y$ for $V \geq 0$. The following procedures have to be followed to simplified the algorithm developed

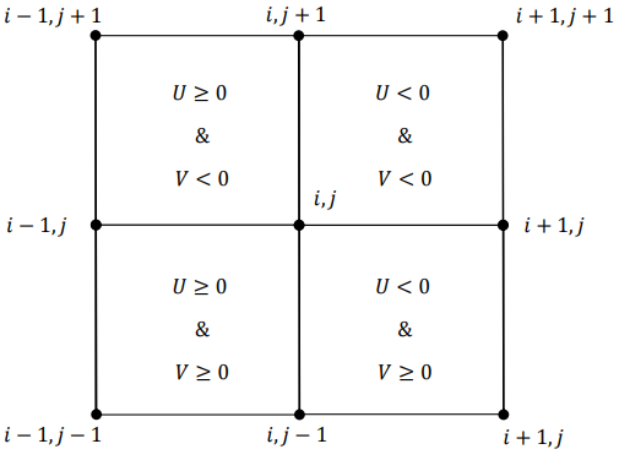

Fig. 5. Meshing in two dimensional CIP

$$isgn = sign(U)$$
$$jsgn = sign(V)$$
$$im1 = i - isgn$$
$$jm1 = j - jsgn$$
$$e_i = \theta_{i+1,j} - \theta_{i,j}$$
$$e_j = \theta_{i,j+1} - \theta_{i,j}$$

Eq. (102)-(104) will be solved using those coefficients

$$B8_{i,j} = \theta_{i,j} - \theta_{im1,j} - \theta_{i,jm1} + \theta_{im1,jm1} \tag{105}$$

$$B1_{i,j} = \frac{-2(\theta_{im1,j} - \theta_{i,j}) + (\partial_X\theta_{im1,j} + \partial_X\theta_{i,j})\Delta X \times (-isgn)}{\Delta X^3 \times (-isgn)} \tag{106}$$

$$B2_{i,j} = \frac{A8_{i,j} - (\partial_X\theta_{i,jm1} - \partial_X\theta_{i,j})\Delta X \times (-isgn)}{(\Delta X^2\Delta Y) \times (-jsgn)} \tag{107}$$

$$B3_{i,j} = \frac{3(\theta_{im1,j} - \theta_{i,j}) - (\partial_X\theta_{im1,j} + 2\partial_X\theta_{i,j})\Delta X \times (-isgn)}{\Delta X^2} \tag{108}$$

$$B4_{i,j} = \frac{-A2_{i,j}(\Delta X^2) + (\partial_Y\theta_{im1,j} - \partial_Y\theta_{i,j})}{(\Delta X) \times (-isgn)} \tag{109}$$

$$B5_{i,j} = \frac{-2(\theta_{i,jm1} - \theta_{i,j}) + (\partial_Y\theta_{i,jm1} + \partial_Y\theta_{i,j})\Delta Y \times (-jsgn)}{\Delta Y^3 \times (-jsgn)} \tag{110}$$

$$B6_{i,j} = \frac{A8_{i,j} - (\partial_Y\theta_{im1,j} - \partial_Y\theta_{i,j})\Delta Y \times (-jsgn)}{(\Delta X\Delta Y^2) \times (-isgn)} \tag{111}$$

$$B7_{i,j} = \frac{3(\theta_{i,jm1} - \theta_{i,j}) - (\partial_Y\theta_{i,jm1} + 2\partial_Y\theta_{i,j})\Delta Y \times (-jsgn)}{\Delta Y^2} \tag{112}$$

2.5 Boundary Condition

The flow in channel is having fully developed flow and the wall of channel is assumed to have adiabatic properties. The cavity has three different walls and they are categorized as shown in Figure 6 where left wall is the vertical left wall of cavity, bottom wall is horizontal wall of the cavity and right wall is the vertical wall of the cavity. For mixed convection one of the walls is remain at constant heat flux where in the code's programmes, ΔT is unity for constant heat flux and ΔT is zero for other walls. The summary of the different heated wall is shown in Table 1. For mixed convection flow, Re will remain constant for all simulation which is at 100. Study on the effect of aspect ratio will also be included in this study.

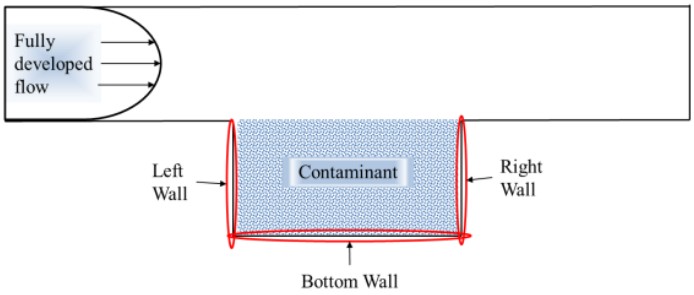

Fig. 6. Sketch of numerical geometry

Table 1
Boundary condition for different heated wall analysis

Constant heat flux location	Temperature boundary condition		
	Left wall	Bottom wall	Right wall
Left wall	Constant heat flux	Adiabatic	Adiabatic
Bottom wall	Adiabatic	Constant heat flux	Adiabatic
Right wall	Adiabatic	Adiabatic	Constant heat flux

The Richardson number, Ri is a dimensionless parameter which will be used in this numerical analysis. In general, forced convection is more dominant in the flow system if Ri less than unity. Mixed convection happens when Ri equal to unity and natural convection flow happen when Ri greater than unity. It may be noted that usually the forced convection is large relative to natural convection except in the case of extremely low forced flow velocities [24]. The equation for Ri is as below. In this study, Gr = 1000, 10 000 and 100 000 will be used as case study for constant Re=100. These values are used to study the effect of forced convection flow, mixed convection flow and natural convection flow to the contaminant removal process. The details of Ri used is as shown in table 2.

$$Ri = \frac{Gr}{Re^2} \tag{113}$$

Table 2
Types of the flow used in numerical simulation

Reynolds number, R_e	Grashof number, G_r	Richardson number, R_i	Type of flow
100	1000	0.1	Forced convection
100	10000	1.0	Mixed convection
100	100000	10	Natural convection

It is important to set a clear selection of convergence criteria. There are many ways to choose on how to stop an iteration loop. Some of research only required the simulation to run until the fluid flow steady and so they stop the simulation when the velocity of fluid at all nodes has no change. In this research, two variables were chosen as parameter to stop the simulation which is stream function and vorticity. Previous calculation of stream function and vorticity will be deducted to current calculation so that if this value is less than 10^{-9}, the simulation will stop. It is simpler to express them as

$$|\Psi^{n+1} - \Psi^n| \,\&\, |\Omega^{n+1} - \Omega^n| \leq 10^{-9} \tag{114}$$

For stability analysis, Courant number should be less than one [25]. This is need to determine the spatial derivative for coding purposes and time marching for the simulation codes. Courant number, C should be less than 1 and as shown in Eq. (115).

$$\frac{c\Delta T}{\Delta X} < 1 \tag{115}$$

3. Results

3.1 Numerical Results in Isothermal Condition

Flow over cavity was simulated using Constrained Interpolated Profile method (CIP) to solve advection part of Navier- Stokes equations and central difference to solve non-advection part of the equations. Reynolds number of 100 to 1000 is used to simulate flow structure inside the cavity for aspect ratio three and aspect ratio four to validate with experiment result obtained earlier.

Afterwards, the results and discussion on numerical simulation on flow over cavity at aspect ratio 1, 2, 3, and 4 for Reynolds number 50, 100, 200, 400 and 1000 will be discussed about their flow behaviour and flow characteristic.

3.1.1 Numerical results of flow structure in the cavity

Figure 7 and 8 shows flow structure for aspect ratio 1-4 at steady state at various Reynolds number. For AR=1, it is shows that only single vortex formed inside cavity for all Re but the centre of vortex is moving towards right side of cavity as Re increase. This is due to stronger shear produced at the shear layer on top of cavity as Re increase and thus creating clockwise vortex with centre of vortex moving to the right of cavity. Similar to AR = 2 but at Re = 1000, secondary vortex with counter clockwise direction is created. This is similar to AR = 3 and AR = 4 where secondary vortex is created due to higher Reynolds number. For AR = 4, Re = 1000, two secondary vortex is created instead of one because of larger aspect ratio of cavity provide more space for main vortex to rotate inside cavity. It is also need to emphasize that all of cavity flow is an open type except AR = 4, Re = 50. Slower flow and larger cavity aspect ratio will let the main flow to enter the cavity to the bottom without creating shear layer at end of cavity.

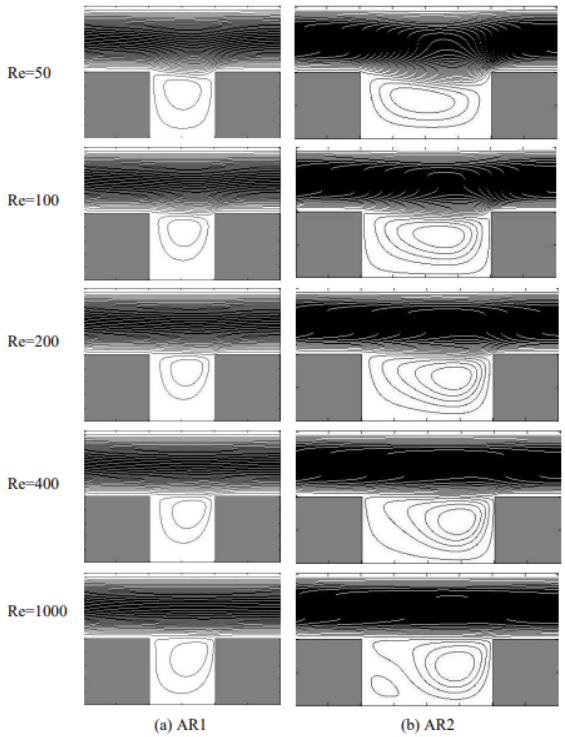

Fig. 7. Flow structure by numerical simulation for various Re for (a) aspect ratio 1 and (b) aspect ratio 2

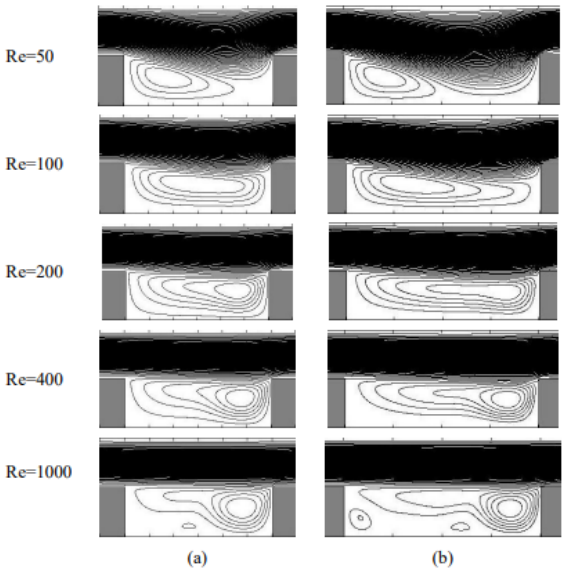

Fig. 8. Flow structure by numerical simulation for various Re for (a) aspect ratio 3 and (b) aspect ratio 4

4. Conclusions

Contaminant removal from square cavity has been studied by using numerical study to simulate transient removal of contaminant for isothermal and mixed convection flow. Constrained Interpolated Profile (CIP) method is used for solving advection term of momentum equation and central difference is used to solve non-advection term of momentum equation to simulate flow

behaviour inside cavity. The numerical studies include different aspect ratios (AR), 1 to 4, various Reynolds numbers (Re), 50 to 1000. It was found that slower flow and larger cavity aspect ratio will let the main flow to enter the cavity to the bottom without creating shear layer at end of cavity.

Acknowledgement
This research was not funded by any grant.

References

[1] Bo, A. N., F. Mellibovsky, J. M. Bergadà, and W. M. Sang. "Towards a better understanding of wall-driven square cavity flows using the lattice Boltzmann method." *Applied Mathematical Modelling* 82 (2020): 469-486.
[2] Garcia, F., C. Trevino, J. Lizardi, and L. Martínez-Suástegui. "Numerical study of buoyancy and inclination effects on transient mixed convection in a channel with two facing cavities with discrete heating." *International Journal of Mechanical Sciences* 155 (2019): 295-314.
[3] Pastur, Luc, François Lusseyran, Jérémy Basley, and Christelle Douay. "Self-sustained oscillations of open cavity flows: when the inner flow dynamics couple to the shear-layer oscillations." In *FIV2018 Conference*. 2018.
[4] Bilgin, Berker, Jianbin Liang, Mladen V. Terzic, Jianning Dong, Romina Rodriguez, Elizabeth Trickett, and Ali Emadi. "Modeling and analysis of electric motors: State-of-the-art review." *IEEE Transactions on Transportation Electrification* 5, no. 3 (2019): 602-617.
[5] Setareh, Milad, Majid Saffar-Avval, and Amir Abdullah. "Heat transfer enhancement in an annulus under ultrasound field: A numerical and experimental study." *International Communications in Heat and Mass Transfer* 114 (2020): 104560.
[6] Cao, Zhixiang, Yi Wang, Chao Zhai, and Meng Wang. "Performance evaluation of different air distribution systems for removal of concentrated emission contaminants by using vortex flow ventilation system." *Building and Environment* 142 (2018): 211-220.
[7] Sahak, Ahmad Sofianuddin A., Nor Azwadi Che Sidik, Siti Nurul Akmal Yusof, and Mahmoud Ahmed Alamir. "Numerical Study of Particle Behaviour in a Mixed Convection Channel Flow with Cavity using Cubic Interpolation Pseudo-Particle Navier-Stokes Formulation Method." *Journal of Advanced Research in Numerical Heat Transfer* 1, no. 1 (2020): 32-51.
[8] Mary Gannon, (2018), 'Hydraulic system contamination: causes and solutions'. Retrieved from https://www.mobilehydraulictips.com/hydraulic-systemcontamination-causes-and-solutions/
[9] Grinis, Lionid, and Eli Korin. "Hydrodynamic method for cleaning inner surfaces of pipes." *Chemical Engineering & Technology: Industrial Chemistry-Plant Equipment-Process Engineering-Biotechnology* 20, no. 4 (1997): 277-281.
[10] Zain A. A. M, (2012), "Contaminant removal from rectangular shaped pipeline joints using constrained interpolated profile method". Masters thesis, Universiti Teknologi Malaysia,
[11] Fang, Lih-Chuan. "Effect of mixed convection on transient hydrodynamic removal of a contaminant from a cavity." *International journal of heat and mass transfer* 46, no. 11 (2003): 2039-2049.
[12] Al-Shehri, Saleh A. "Cooling computer chips with cascaded and non-cascaded thermoelectric devices." *Arabian Journal for Science and Engineering* 44, no. 11 (2019): 9105-9126.
[13] Ferziger, Joel H., Milovan Perić, and Robert L. Street. *Computational methods for fluid dynamics*. springer, 2019.
[14] Abdelmassih, Gorg, Anton Vernet, and Jordi Pallares. "Steady and unsteady mixed convection flow in a cubical open cavity with the bottom wall heated." *International Journal of Heat and Mass Transfer* 101 (2016): 682-691.
[15] YADOLLAHI, FARSANI ROUHOLLAH, Behzad Ghasemi, and Saiied Mostafa Aminossadati. "Magnetohydrodynamic mixed convection effects on the removal process of fluid particles from an open cavity in a horizontal channel." (2014): 67-74.
[16] Stiriba, Y., F. X. Grau, J. A. Ferré, and A. Vernet. "A numerical study of three-dimensional laminar mixed convection past an open cavity." *International Journal of Heat and Mass Transfer* 53, no. 21-22 (2010): 4797-4808.
[17] Aminossadati, Saiied M., and Behzad Ghasemi. "A numerical study of mixed convection in a horizontal channel with a discrete heat source in an open cavity." *European Journal of Mechanics-B/Fluids* 28, no. 4 (2009): 590-598.
[18] Manca, Oronzio, Sergio Nardini, Khalil Khanafer, and Kambiz Vafai. "Effect of heated wall position on mixed convection in a channel with an open cavity." *Numerical Heat Transfer: Part A: Applications* 43, no. 3 (2003): 259-282.
[19] Manca, Oronzio, Sergio Nardini, and Kambiz Vafai. "Experimental investigation of mixed convection in a channel with an open cavity." *Experimental heat transfer* 19, no. 1 (2006): 53-68.
[20] Manca, Oronzio, Sergio Nardini, and K. Vafai. "Experimental investigation of opposing mixed convection in a channel with an open cavity below." *Experimental Heat Transfer* 21, no. 2 (2008): 99-114.

[21] Lequeurre, Julien, and Alexandre Munnier. "Vorticity and stream function formulations for the 2D Navier–Stokes Eq.s in a bounded domain." *Journal of Mathematical Fluid Mechanics* 22, no. 2 (2020): 15.
[22] Hamid, Aamir, and Masood Khan. "Unsteady mixed convective flow of Williamson nanofluid with heat transfer in the presence of variable thermal conductivity and magnetic field." *Journal of Molecular Liquids* 260 (2018): 436-446.
[23] Sahak, Ahmad Sofianuddin A., Nor Azwadi Che Sidik, and Siti Nurul Akmal Yusof. "Cubic Interpolation Pseudo-Particle Navier-Stokes Formulation Method for Solid Particle-Fluid Interaction in Channel Flow with Cavity." *Journal of Advanced Research in Numerical Heat Transfer* 1, no. 1 (2020): 52-68.
[24] Muhammad, Riaz, M. Ijaz Khan, Mohammed Jameel, and Niaz B. Khan. "Fully developed Darcy-Forchheimer mixed convective flow over a curved surface with activation energy and entropy generation." *Computer Methods and Programs in Biomedicine* 188 (2020): 105298.
[25] Konangi, Santosh, Nikhil K. Palakurthi, and Urmila Ghia. "von Neumann stability analysis of first-order accurate discretization schemes for one-dimensional (1D) and two-dimensional (2D) fluid flow Eq.s." *Computers & Mathematics with Applications* 75, no. 2 (2018): 643-665.